Sintering and Crystallite Growth of Nanocrystalline Copper Doped Tin Oxide

C. V. Santilli,[†] S. H. Pulcinelli,[†] G. E. S. Brito,[†,‡] and V. Briois*[,‡]

Instituto de Química, UNESP, P.O. Box 355, 14801-970 Araraquara SP, Brazil, and LURE, Centre Universitaire Paris-Sud, Bât 209D, B.P. 34, 91898 Orsay Cedex, France

Received: October 22, 1998; In Final Form: January 3, 1999

The effect of Cu^{2+} contents and of firing temperature on sintering and crystallite growth of nanocrystalline SnO_2 xerogels was analyzed by thermoanalysis (mass loss (TG), linear shrinkage, and differential thermal analysis (DTA)), X-ray powder diffraction (XRPD), and EXAFS (extended X-ray absorption fine structures) measurements. Samples were prepared by two methods: (a) coprecipitation of a colloidal suspension from aqueous solution containing both Sn(IV) and Cu(II) ions and (b) grafting copper(II) species on the surface of tin oxide gel. The thermoanalysis has shown that the shrinkage associated with the mass loss decreases by increasing the amount of copper. The EXAFS measurements carried out at the Cu K edge have evidenced the presence of copper in substitutional solid solution for the dried xerogel prepared with 0.7 mol % of copper, while for higher concentration of doping, copper has been observed also at the external surface of crystallites. The solid solution is metastable and copper migrates toward the surface during firing. The XRPD and DTA results have shown a recrystallization process near 320 °C, which leads to crystallite growth. The presence of copper segregated near the crystallite surface controls its growth.

I. Introduction

Highly porous tin dioxide films and ceramics are widely used as semiconductor gas sensors due to their low cost and high sensibility to a great number of reducing gases.[1,2] The sensitivity and selectivity of devices are achieved by addition of metals having catalytic properties (Pd, Pt). Recently, it was reported[3] that SnO_2 impregnated with a small amount of CuO is extremely selective to most toxic gases, like H_2S and SO_2. On the other hand, dense SnO_2 has potential application in the manufacturing of stable electrodes, e.g., for aluminum electrolysis and glass melting furnace.[4] For this purpose copper(II) oxide is added in order to improve the sintering ability, ensuring a low porosity of the SnO_2-based ceramic.[5]

Despite the technological interest in Cu(II)-doped SnO_2 ceramics, the role of this additive in the sintering mechanism has been established only for temperatures higher than 950 °C, in which the formation of a liquid phase ensures the densification of SnO_2 ceramics containing small amounts of copper oxide (1 mol %).[6] Between 940 and 1000 °C, densification is controlled by the dissolution process and at higher temperatures the transfer of matter is limited by liquid-state diffusion.[6] For sintering temperatures lower than 940 °C, several mechanisms have been proposed to explain the improvement of the densification of SnO_2 due to copper oxide addition. Some authors[7] assumed that solid-state bulk diffusion is activated by the formation of lattice defects due to the dissolution of the Cu(II) in the SnO_2 network, whereas others attributed the densification to a fast copper distribution on the SnO_2-based grain surface. Furthermore, there are clear experimental evidences that copper additions could stabilize the ultrafine particles[8] and pores[9] of SnO_2, due to the decrease of the grain boundary mobility.

This paper is a result of our continuous effort[9−12] to understand the sintering process of nanocrystalline SnO_2 materials prepared by the sol−gel route. We have evidenced, by extended X-ray absorption fine structures (EXAFS) and X-ray powder diffraction (XRPD), that the dried gel is formed by a few nanometer crystalline domains with the incipient cassiterite structure.[10] The dehydration, which takes place between 100 and 250 °C, causes an amorphization of the cassiterite structure due to condensation reactions involving OH groups located at the surface of the same crystallite.[11] This feature gives rise to the rupture of the xerogel network, evidenced by micropore formation,[12] favoring the microstructural rearrangements and densification. Over 250 °C the oxolation reaction involving OH groups at the surface of adjacent crystallites improves the rebuilding of the long-range crystalline order and densification. Furthermore, between 300 and 700 °C continuous coagulation of crystallites occurs leading to grain and pore growth.[11,12] The addition of Cu(II) hinders the micropore formation and decreases the kinetics of pore coarsening as the concentration of doping increases.[9] The analysis of the Porod region of the SAXS curves recorded at 500 °C suggests that addition of Cu(II) up to 0.7% leads to the formation of a nonhomogeneous solid solution, the Cu(II) being preferentially located near the crystallite surface. For higher concentrations, the roughness of the crystallites increases with the time of isothermal treatment, which was attributed to a demixing of a copper rich phase.[9] This interpretation is in agreement with the recent EXAFS study carried out for 10 mol % of copper doped SnO_2 xerogels performed by Davis and co-workers[13] that has shown that doping atoms move to the surface region of the crystallites during the heating. Furthermore similar evidence of copper in SnO_2 solid solution and of adsorbed copper at the surface of crystallites has been obtained from EPR measurements.[14]

Our objectives in this paper were 2-fold: first, to obtain more information about the effect of different additions of Cu(II) on the nanostructure evolution during thermal treatment of SnO_2 xerogels, and second, to determine the copper environment of nanocrystalline SnO_2 matrix by using EXAFS measurements at the Cu and Sn K edges.

2. Experimental Section

2.1. Samples Preparation. $SnCl_4 \cdot 5H_2O$ (BDH) and $CuCO_3 \cdot Cu(OH)_2$ (Merck) were used to prepare SnO_2 aqueous colloidal

* Corresponding author: e-mail, briois@lure.u-psud.fr.
† Instituto de Química.
‡ LURE.

10.1021/jp984129v CCC: $18.00
Published on Web 03/20/1999

suspensions containing different quantities of copper (between 0.7 and 5.0 mol %), according to ref 9. The SnO_2:Cu hydrosols were prepared from the aqueous solutions, precipitated by aqueous ammonium at pH = 11, which were dialyzed against bidistilled water in order to eliminate as much NH_4^+ and Cl^- as possible. Transparent aqueous suspensions were poured into a Teflon beaker containing a mixing of liquid paraffin and chloroform. Due to the lower density of the hydrosol, it spreads over the bath and remains on the surface, resulting in a large area of evaporation. The sol−gel transition was obtained at a critical concentration of SnO_2 (0.42 mol·L^{-1}) achieved by partial evaporation of water at 45 °C. During drying at room temperature, a fragile sheet is formed, which is peeling by dissolving the paraffin film remaining between the sample and the beaker, by washing with hexane. The resulting glasslike monolithic xerogels were isothermally treated at 110, 300, and 600 °C during 30 min. The copper content in the xerogels was determined by ICP/AES technique. For comparison purposes, we have prepared samples of copper chloro complexes chemically grafted (12 mol %) onto an SnO_2 surface, according to ref 3.

2.2. Thermoanalysis Measurements. Simultaneous thermogravimetric and differential thermoanalysis on the monolithic xerogel were carried out in a TGA-DTA-TA Instrument. The linear shrinkage during heating of the monolith was measured in a Netch dilatometer. Both sets of experiments were carried out between 30 and 700 °C at heating rate of 4 °C·min^{-1} under synthetic air flux.

2.3. X-ray Powder Diffraction and EXAFS. Ex situ XRPD measurements have been performed on samples isothermally heated with a Siemens D5000 powder diffractometer using the Ni filtered Cu $K\alpha_2$ radiation. A high-temperature chamber (HTP-Anton Paar) was used for in situ isothermal XRPD measurements between 50 and 700 °C. The patterns were collected 20 s after each increment of 20 °C on the sample temperature. A one-dimensional position-sensitive X-ray detector was used for fast $\theta-2\theta$ scan (typically 1 min per XRPD pattern). For assessment of mean crystallite size and microstrain, the $K\alpha_1$ and $K\alpha_2$ doublet deconvolution and background corrections were performed by fiting the X-ray profile with a pseudo-Voigt function (PVF).[15] The Stokes' instrumental broadening correction, the mean crystallite size, and the microstrain were deduced by using Fourier coefficient calcutated from PVF.[15]

EXAFS measurements were carried out at room temperature using the EXAFS I spectrometer equipped with a channel-cut Si (331) monochromator at the synchrotron DCI source (1.85 GeV and 300 mA) at LURE, Orsay, France. Sn K edge (29200 eV) EXAFS spectra were collected under 1200 eV energy (2-s acquisition time per 4-eV energy step) in transmission mode using ionization chambers filled with Krypton as detectors. Copper K edge (8979 eV) measurements were performed in transmission or fluorescence mode depending on the copper concentration. Fluorescence spectra have been collected by using a Ge solid-state detector under a 800-eV energy range with 10-s acquisition time per 2-eV energy step. Several acquisitions (between 5 and 12 spectra depending on the Cu concentration) were carried out on the same sample to improve the signal-to-noise ratio. Samples were ground and mixed with cellulose before being pressed into pellets. The quantity of powdered samples was chosen to obtain edge jumps in the transmission mode of about $\Delta\mu x \approx 1$. Crystalline SnO_2 and CuO samples were used as references at the Sn and Cu K edges, respectively. This CuO reference was recorded both in transmission and fluorescence mode (nominal 5 mol % of CuO mixed with SnO_2 crystalline powder).

All the EXAFS spectra were treated by using the classical plane-wave single scattering approximation.[16] The treatment has been performed with the "EXAFS pour le MAC" program developed by Michalowicz.[17] At the Sn K edge, the EXAFS oscillations were analyzed according to the procedure fully described in ref 10. Structural parameters reported in Table 1S, Supporting Information, were determined by a least square fitting procedure by using the Round Midnight program[17] as explained in ref 18. The accuracy in their determination is typically 1% for the interatomic distances, 15% for both the coordination number and Debye−Waller factor. At the Cu K edge, the main lines of the procedure are summarized here. After atomic absorption removal and normalization, the $k^3\chi(k)$ weighted EXAFS signal was Fourier transformed to R distance space, using the 3.4−12.8 $Å^{-1}$ Kaiser apodization window with $\tau = 2.5$. The contribution of the first shell of oxygen neighbors was extracted by a back Fourier transform in R space and then fitted by using experimental phase and amplitude functions extracted from the CuO reference. This was done backtransforming the first peak of its Fourier transform (FT) and setting $N = 4$, $R = 1.96$ Å, and $\sigma = 0.070$ Å.[19] This Debye−Waller factor was determined by fitting first the filtered peak for the reference, using theoretical functions as reported in the McKale's tables.[20] This approach allows one to obtain an experimental amplitude function not convoluted with the Debye−Waller term, but still convoluted with the mean free path. Oxygen coordination numbers, Debye−Waller factors, and Cu−O distances for samples were obtained by using the least-squares fitting procedure available with Round Midnight. The error bars specified in Table 1 (Results section) were determined from the average standard deviation $\epsilon(k)$ for a set of EXAFS spectra recorded for the same sample. We used the empirical rule proposed by Andreatta et al.[21] to correctly estimate the average standard deviation from a finite number of spectra. The quality of the fit is given by the value of the reduced χ-squared $\Delta\chi v^2$ as defined in ref 22. For the copper oxide reference and doped xerogels, contributions at longer distances cannot be isolated simply because of the occurrence of a different set of atoms (Cu, O, and Sn) at similar distances. For the Cu−Cu contribution, we checked theoretical amplitude and phase functions[20] on the CuO reference in order to determine electronic parameters such as the Γ factor ($\Gamma = 0.4$ $Å^{-2}$) related to the mean free path λ of the photoelectron ($\lambda = k/\Gamma$) and the threshold energy E_0 used to convert the EXAFS signal from energy to wavevector by the relation $k = ((2m/\hbar^2)(E - E_0))^{1/2}$. Starting from these values of Γ and E_0 we verified that the contribution at longer distances for the doped xerogels cannot be adjusted by using only Cu−O and Cu−Cu contributions. Satifactory fits can be obtained by considering two Cu−Sn contributions with Cu−Sn distances equal to 3.12 and 3.63 Å, respectively. This result is in agreement with the SAXS result,[9] which indicated the formation of a solid solution. Unfortunately, the lack of a reference with a Cu−Sn contribution does not allow one to obtain an accurate number of tin neighbors using the conventional route, and we changed our strategy by using ab initio calculations available with the FEFF6 code[23] in the single scattering framework as presented in the Discussion section.

3. Results

The curves of thermogravimetry, differential thermoanalysis, and thermodilatometry are shown in Figure 1, parts a, b, and c, respectively. Undoped and doped samples exhibit, up to 110

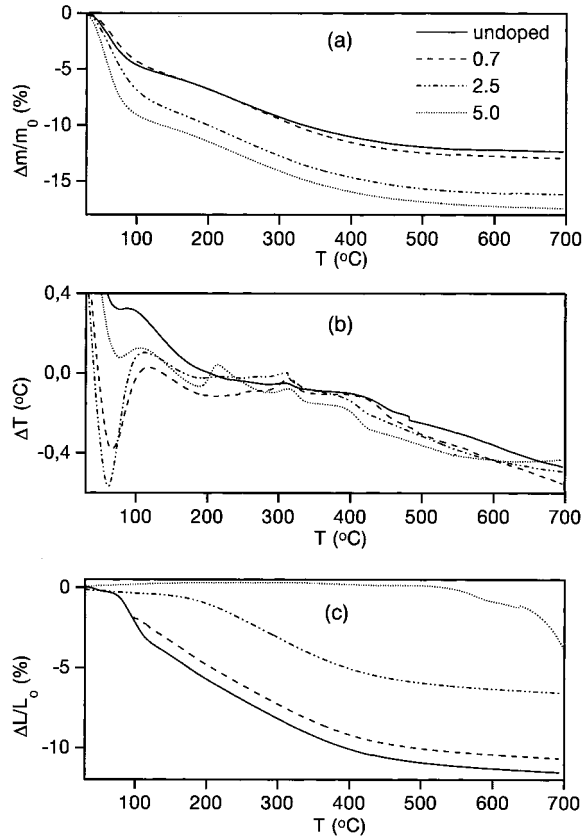

Figure 1. (a) Thermogravimetry, (b) differential thermoanalysis, and (c) thermodilatometry curves for undoped and doped (0.7, 2.5, and 5.0 mol %) SnO_2 xerogels.

°C, an endothermical effect followed by marked mass loss due to the liberation of adsorbed water. The amount of adsorbed water increases with Cu-doping, reaching a maximum for the sample containing 5.0% Cu, whereas the linear shrinkage is suppressed, increasing the amount of doping. Between 110 and 500 °C all samples exhibit a continuous mass loss. As first proposed by Sharygin[24] and confirmed by infrared analysis,[25] this mass loss is due to dehydroxylation of the particle surface and boundaries. In this temperature domain, undoped and doped samples show practically the same mass loss (7%), meanwhile, the linear shrinkage decreases with doping, being almost suppressed for the sample containing 5% Cu. DTA curves present a small exothermic effect with a maximum temperature near 320 °C. From the dependence between the maximum temperature and the drying condition, Sharygin[24] attributed this effect to oxolation reactions. However, we have shown that the crystallinity of the pure xerogel is a function of the drying process[10] and that heating of compacted xerogels (from 110 to 250 °C) leads to an amorphization of the incipient cassiterite structure.[11] A recovering of the crystallinity was observed after thermal treatment at 400 °C. From this behavior together with the structural results presented in the following, we propose that this exothermic effect may be due to a recrystallization process. The 5% Cu-doped sample shows another exothermic peak with a maximum near to 210 °C. This effect depends on the Cu amount and may results from the formation of a Cu-rich phase.Two exothermal peaks, at 375 and 454 °C, were also observed by Fang et al [26] and attributed to the formation and decomposition of $CuSnO_3$, respectively.

A typical evolution of the diffraction patterns measured in situ during heating of undoped SnO_2 powdered xerogel is shown in Figure 1S. Diffuse peaks corresponding to planes (110), (101), and (211) of the cassiterite structure are observed for the dried sample, characteristic of nanocrystalline materials. As the temperature increases from 350 to 750 °C the peaks become narrower and more intense, characterizing crystallite growth. Analogous behavior has been observed for Cu-doped SnO_2 and copper chloro complexes grafted xerogels. The formation of any secondary crystalline phase has been observed during heating for Cu-doped samples, whereas for the grafted ones a very low intensity $^{-}1\ 1\ 0$ peak of CuO could be observed after firing at 700 °C.

Figure 2 shows the evolution of crystallite size and microstrain with firing temperature for undoped, doped, and grafted samples for [101] and [110] for the early sintering stage (1 min) determined from in situ XRPD experiments. Above 400 °C, a continuous crystallite growth and a decrease of the microstrains are observed for all the samples at both directions. The crystallite size measured along [101] is almost independent of the copper concentration and equal to the size measured for the undoped xerogel, except for the grafted sample. For the 0.7% copper doped sample, the presence of a peak on the crystallite size and microstrain versus T curve has been observed with a maximum position at ≈340 °C, *i.e.*, close to the temperature at which the exothermic effect has been observed by DTA (Figure 1). This result is in agreement with the recrystallization process proposed before. It is important to note that along [110], the crystallite size is nearly constant until 500 °C and smaller than the size developed along [101]. Above this temperature, the crystallite growth along this direction seems to be controlled by the copper concentration.

Figure 3 shows the dependence with the dopant concentration on the crystallite size and microstrain for the later sintering stage (30 min) at 600 °C obtained from ex situ XRPD measurements. Contrary to the results observed for the early sintering stage, the crystallite size measured at the later stage for both directions is controlled by the addition of copper. A minimal crystallite size is observed for the 0.7% copper amount. For higher dopant concentrations, the crystallite size remains nearly constant. The doped xerogels present a microstrain rate almost constant but the values are higher than measured for the undoped sample. Furthermore, we observe that the early (Figure 2) and later (Figure 3) time periods of sintering are characterized by very different crystallite sizes and nearly equal microstrain rates.

Figure 4 compares the Fourier transform of the EXAFS spectra recorded at Sn K edge for undoped, doped, and grafted xerogels dried and fired at 300 and 600 °C. All the samples present a FT characteristic of the cassiterite structure with two main peaks located in the range $1 < R < 2.2$ Å and $2.4 < R < 4.0$ Å. The first peak corresponds to the contribution of the first oxygen coordination shell around tin, the second broad one mainly to tin−tin contributions. The intensity reduction of the second contribution of the FTs for xerogels compared to the intensity of the crystalline reference has been correlated previously to the nanocrystalline size.[10] From the comparison of the FT of dried samples containing copper with the undoped dried xerogel, it appears that the addition of copper does not change considerably the local order around tin. Nevertheless, we observe an increase of the intensity of the peak located at ≈2.9 Å by doping the xerogel, this effect being more important for the 0.7%. This feature has been attributed previously[10] to a preferential growth along the *c* axis during drying, which is dependent on the ionic strength of the solution. When the temperature is raised, we notice a decrease in the amplitude of the second peak with an increase in copper doping. This effect is particularly marked for the grafted sample at 600 °C. This

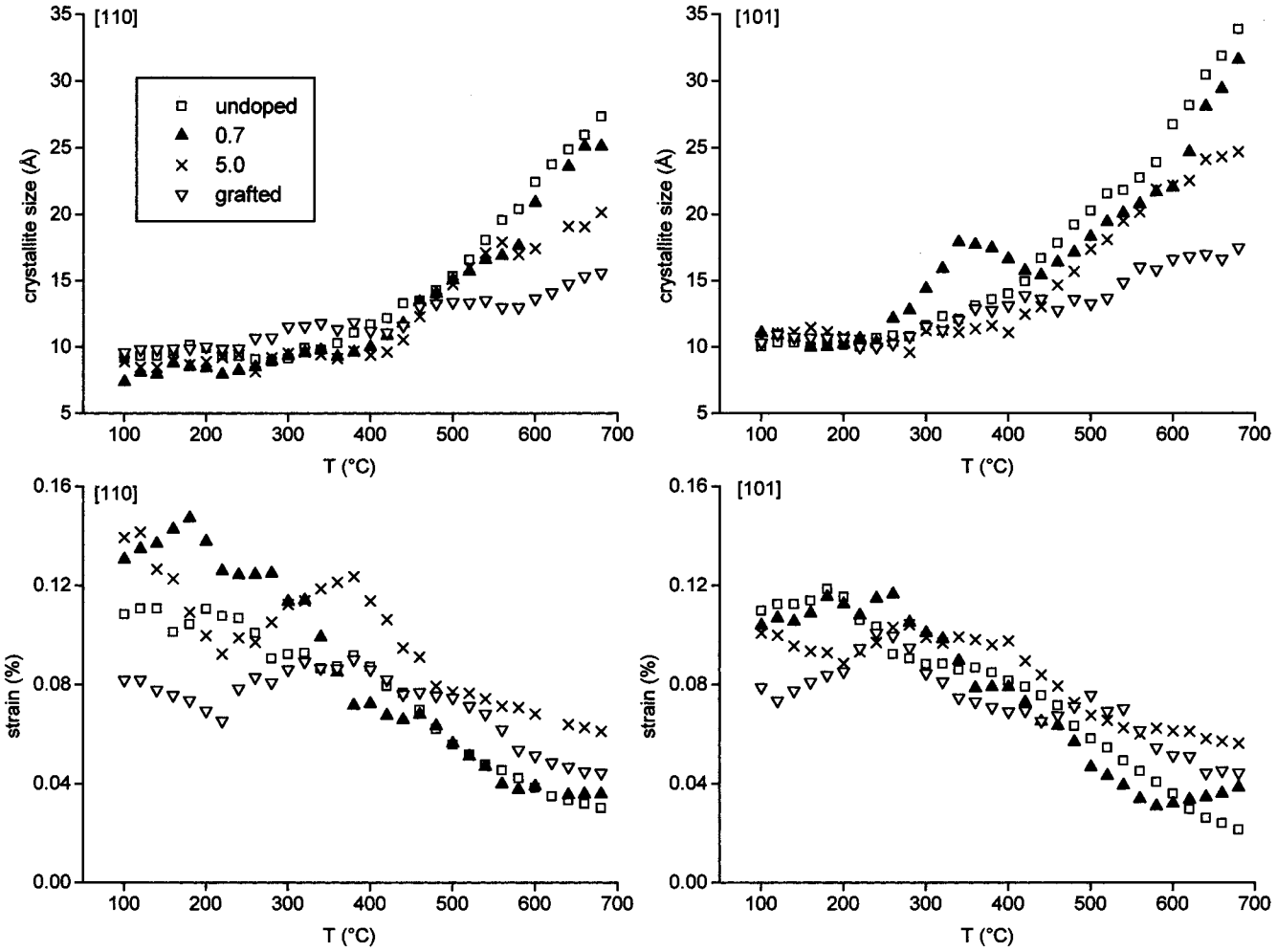

Figure 2. Evolution of the crystallite size (upper panels) and microstrain (lower panels) for undoped, doped (0.7, 2.5, and 5.0 mol %), and grafted SnO_2 xerogels during the early time period of sintering (1 min) determined from [110] (left) and [101] (right) peak profiles.

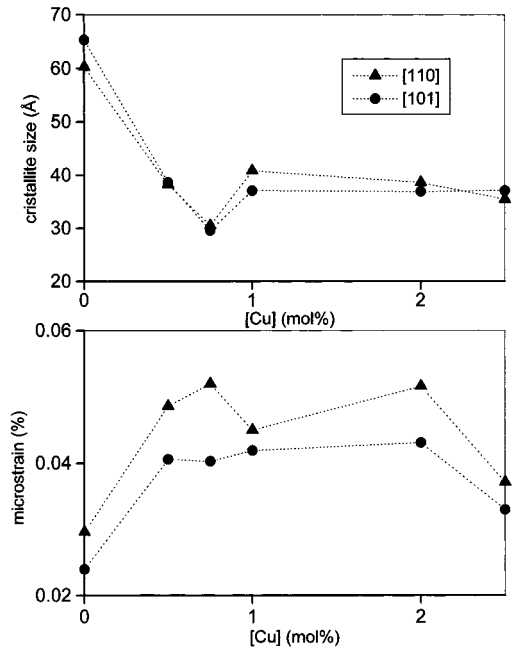

Figure 3. Evolution of the crystallite size and microstrain for undoped and doped (0.7, 2.5, and 5.0 mol %) SnO_2 xerogels for the later time period of sintering (30 min) at 600 °C.

can be attributed to the increase of the Debye−Waller factor or to the decrease of coordination number. Irrespected to the better interpretation, this behavior indicates that the addition of copper disturbs the network of tin atoms with respect to the undoped situation. Selected structural parameters determined by a least-squares fitting procedure of the filtered EXAFS signal are gathered in Table 1S. The Sn−O distances for the first coordination shell are 2.06 ± 0.01 Å, whereas the Sn−Sn distances for the first and second nearest tin contributions are 3.17 ± 0.02 and 3.72 ± 0.02 Å. It is important to note that the coordination numbers and Debye−Waller values of samples dried and fired at 300 °C for the Sn−Sn contributions (Table 1S) are almost independent of copper concentration. The decrease of intensity of the second peak observed with increasing copper concentration in the FTs of doped samples fired at 600 °C is due both to an increase of the Debye−Waller factors (from 0.046 to 0.059 Å for the shell at 3.17 Å and from 0.061 to 0.068 Å for the shell at 3.72 Å) and to a decrease of the mean Sn−Sn coordination numbers (from 7.6 to 6.2 for the shell at 3.72 Å) in agreement with the crystallite size determined by XRD for doped xerogels fired at 600 °C. Furthermore, we can note the clear increase of Debye−Waller factors for the oxygen coordination shell when the samples are doped and fired at 600 °C (from 0.046 to 0.060 Å), indicating that the oxygen network is perturbated by the addition of copper.

For different Cu-dopant concentration, the Cu K edge EXAFS spectra for samples fired at 300 °C are presented in Figure 5 a) and compared to the EXAFS spectra of grafted samples. The shape of the EXAFS spectra depends clearly on the dopant concentration: the bigger the doping concentration the smaller

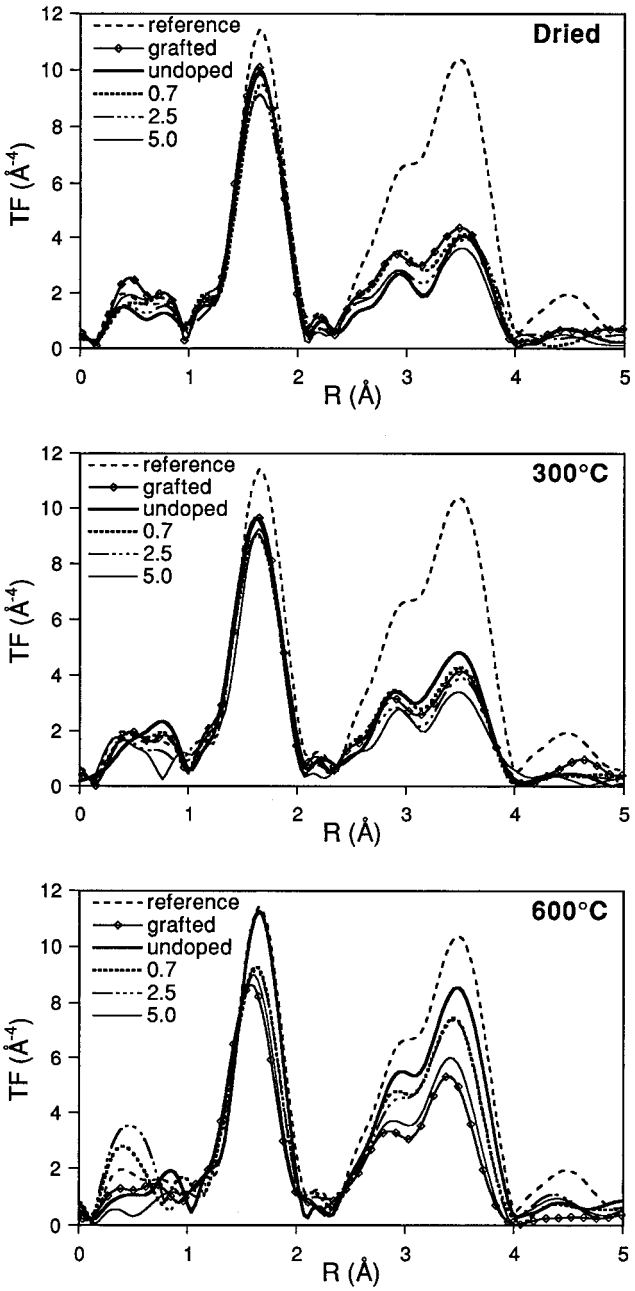

Figure 4. Fourier transforms of the EXAFS signals recorded at the Sn K edge for undoped, doped (0.7, 2.5, and 5.0 mol %), and grafted SnO_2 xerogels as a function of the temperature of treatment.

the intensity of the sharp-pointed contribution at low *k* values for the first oscillation. As a consequence, the spectra acquire progressively the shape of the copper grafted xerogel. This is evidence of the change in copper local order with the dopant concentration.

The FTs of the EXAFS spectra presented in Figure 5a are given in Figure 5b. The change in the shape of the EXAFS signals observed with an increasing dopant concentration corresponds on the FTs to a drastic change in the intensity of the second broad contribution located between 2 and 4 Å. Structural parameters determined by the least-squares fit of the filtered EXAFS signals for the first contribution are gathered in Table 1. We observe first a decrease of the oxygen coordination number from 6 to 4 when the copper concentration increases and second a significant shift of the copper−oxygen distance from 2.01 to 1.96 Å. For the smallest dopant concentration, the value of 6 as oxygen coordination number together

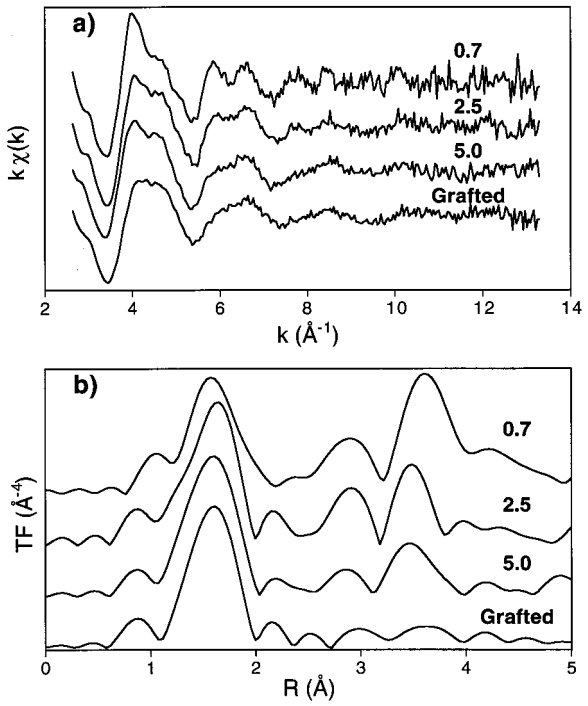

Figure 5. Comparison of (a) the EXAFS signals recorded at the Cu K edge and (b) the corresponding Fourier transforms for doped (0.7, 2.5, and 5.0 mol %) and grafted SnO_2 xerogels fired at 300 °C for 30 min.

TABLE 1: Selected Structural Parameters for the Oxygen Contribution Determined by a Least Square Fitting Procedure of the EXAFS Filtered Signal[a]

samples		dried	300 °C	600 °C
0.7 mol %	*N*	4.8 ± 0.9	6.1 ± 1.1	4.8 ± 0.6
	σ (Å)	0.091 ± 0.039	0.112 ± 0.017	0.094 ± 0.015
	R (Å)	1.997 ± 0.015	2.012 ± 0.020	1.990 ± 0.012
	$\chi v2$	0.02	0.02	0.05
2.5 mol %	*N*	5.9 ± 0.6	4.6 ± 0.4	4.6 ± 0.5
	σ (Å)	0.108 ± 0.008	0.095 ± 0.011	0.084 ± 0.009
	R (Å)	1.968 ± 0.009	1.979 ± 0.008	1.970 ± 0.007
	$\chi v2$	0.32	0.14	0.26
5.0 mol %	*N*	4.4 ± 0.3	3.9 ± 0.3	3.6 ± 0.3
	σ (Å)	0.086 ± 0.009	0.082 ± 0.009	0.084 ± 0.009
	R (Å)	1.979 ± 0.007	1.975 ± 0.007	1.970 ± 0.007
	$\chi v2$	0.04	0.35	0.17
grafted	*N*	3.5 ± 0.6	3.2 ± 0.4	3.5 ± 0.6
	σ (Å)	0.079 ± 0.010	0.070 ± 0.016	0.084 ± 0.017
	R (Å)	1.967 ± 0.016	1.966 ± 0.018	1.962 ± 0.018
	$\chi v2$	0.46	0.22	0.30

[a] The Γ (in Å^2) and E_o (in eV) parameters, determined for the crystalline CuO reference, were kept constant and equal to 0.0 and 8 981 (2).

with the fact that the second broad contribution looks like the main Sn−Sn contributions observed at the Sn K edge suggests strongly that the copper substitutes tin in the cassiterite structure. Furthermore, the changes both in the oxygen coordination number and shape of the second contribution in the FTs evidence a demixed copper phase when the dopant concentration increases.

Figure 6, parts a and b, display the EXAFS spectra and corresponding FT for the xerogel doped 0.7% and isothermally treated during 30 min at different temperatures, respectively. The sharp pointed shape for the first EXAFS oscillation is more pronounced at 300 °C, whereas the second EXAFS oscillation appears better defined with a double structure. Above 300 °C, the first and second EXAFS oscillations become structureless. This loss of structures is more pronounced for the higher doped

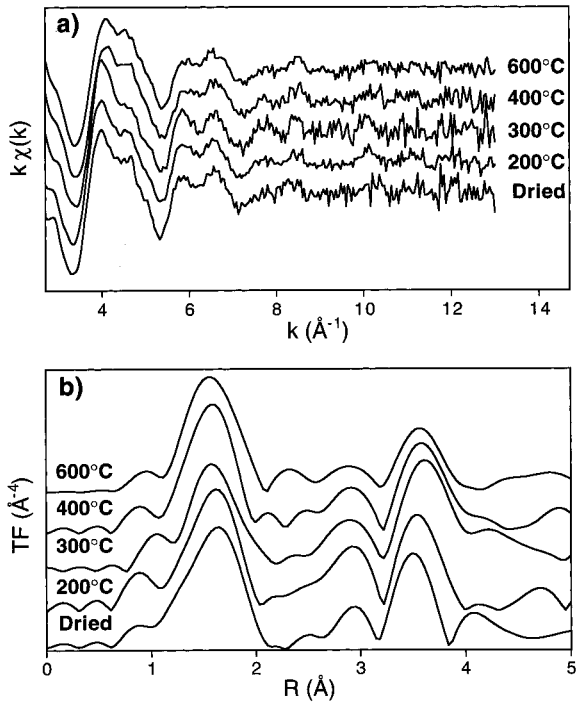

Figure 6. Comparison of (a) the EXAFS spectra recorded at the Cu K edge and (b) the corresponding Fourier transforms for doped (0.7 mol %) SnO_2 xerogels isothermally treated (30 min) at different temperatures.

samples, for which the spectra acquire a similar shape to the spectrum of the grafted sample (Figure 5). Regardless of the temperature of heat treatment, the spectral shape of the grafted samples is unmodified. The more remarkable modifications on the FTs (Figure 6b) occur on the second broad contribution. In particular, as the temperature increases from 200 to 300 °C, the peak at 3.5 Å is shifted to longer distance and its intensity increases. Above this temperature, the peak remains at the same distance, whereas its intensity decreases.

4. Discussion

4.1. Ab Initio Simulations of Copper Location in the SnO_2 Nanocrystalline Matrix. Taking into account all the previous SAXS results[9] and the present ones obtained for the smallest concentration of dopant, we have a strong evidence of the formation of a solid solution in which tin would be replaced by copper. Nevertheless, recent EPR and EXAFS studies[13,14] have suggested the presence of both substitutional and interstitial solid solutions in Cu-doped SnO_2 xerogels. Furthermore, the modification of the copper environment by increasing the temperature poses the question of movement of the copper toward the surface: formation of an adsorbed layer on the surface, formation of a heterogeneous solid solution near the crystallite surface, or formation of a secondary phase. All these hypotheses were checked by simulating the copper K edge EXAFS spectra, assuming different sites for the copper atom in the cluster of cassiterite structure. Figure 7 represents the modeled copper sites in SnO_2 nanocrystallite used for the simulation of copper in substitutional and interstitial solid solutions. The size of this idealized crystallite is in agreement with the mean size determined by XRPD for dried samples. It has been modeled from three cells developed along the *c* axis and two cells along the *a* and *b* axes. In the calculations, the 6-fold oxygen coordination for tin atoms has been set. For the substitutional solid solution, we distinguish two bulk sites (a, b) both

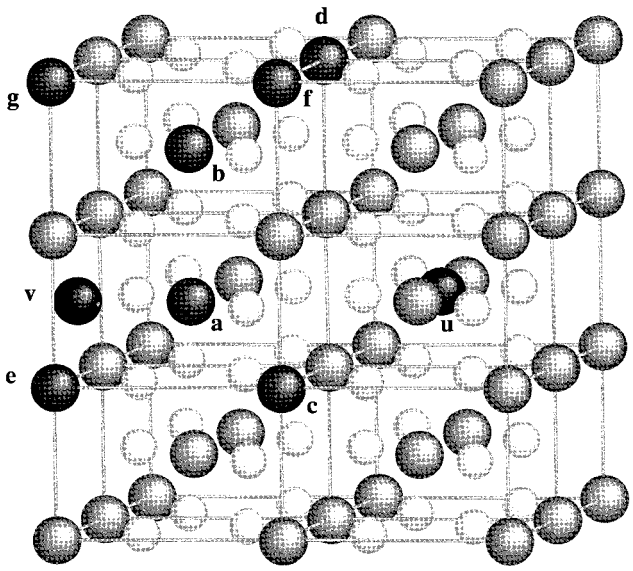

Figure 7. Representation of the different copper substitutional (a−g) and interstitial (u and v) sites in an idealized crystallite of SnO_2 built up from three cells along the *c* axis and two cells along the *a* and *b* axes. The tin sites are displayed by large circles, whereas the oxygen atoms are represented by the smallest ones.

characterized by eight nearest Sn atoms along [111] and five superficial sites (c to g) which are characterized by four, four, two, two, and one nearest Sn atoms located along [111], respectively. For the interstitial case, one bulk site, u, and one superficial site, v, are available, all being characterized by a large distribution of distances. Theoretical calculations were compared to the EXAFS results obtained for the lowest doping concentration, to be sure that the probability of having a copper atom surrounded by another copper atom is negligible: *i.e.*, one site by the cluster is occupied by copper for each calculation. To take into account the significant reduction of Cu−O and Cu−Sn distances determined with Round Midnight on the doped samples with respect to the Sn−O (2.06 Å) and the Sn−Sn distances (3.17 and 3.72 Å) for the cassiterite structure, it was necessary to consider a local strain around the absorbing copper atom. For the substitutional solid solution, a strain relaxation with a Gaussian distribution was assumed, which corresponds typically, in terms of structural contraction, to about 3.0 and 2.3% for the first oxygen coordination shell and for the second and third Sn nearest neighbors, respectively. Due to the Cu−O distance in the first coordination shell (two atoms at 1.74 Å and four atoms at 2.34 Å) characterizing the interstitial sites, the simulated EXAFS signals are out of phase with the experimental one. To obtain an agreement between the phase of the experimental and the simulated curves, it would be necessary to consider a local deformation of the oxygen octahedron of almost 16%. This strong elastic field, if any, gives rise to an unstable structure. Otherwise, if taking into account this hypothetical deformation, it is noteworthy that the shape of the simulated EXAFS oscillations does not correspond to the experimental one. It is demonstrated that the formation of an interstitial solid solution suggested in ref 14 does not hold.

The simulations for the copper in the different substitutional positions are shown in Figure 8 and compared to the experimental EXAFS spectra for the smallest dopant concentration and for the grafted sample, both heating at 300 °C. The sharp pointed shape of the first EXAFS oscillation and split structures on the second one are clearly a fingerprint of a copper atom replacing a tin atom in the bulk (sites a and b). When the copper atom replaces tin at the surface (sites c to g) of the crystallites,

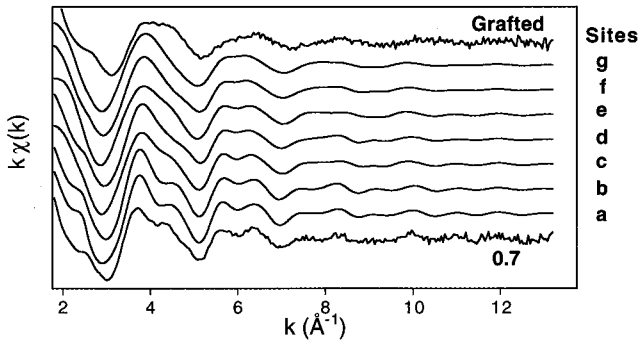

Figure 8. Comparison of the experimental EXAFS spectra recorded at the Cu K edge for doped (0.7 mol %) and grafted SnO_2 xerogels fired at 300 °C for 30 min with ab intio calculations of the EXAFS spectra corresponding to copper atoms located at the different substitutional sites modeled in Figure 7.

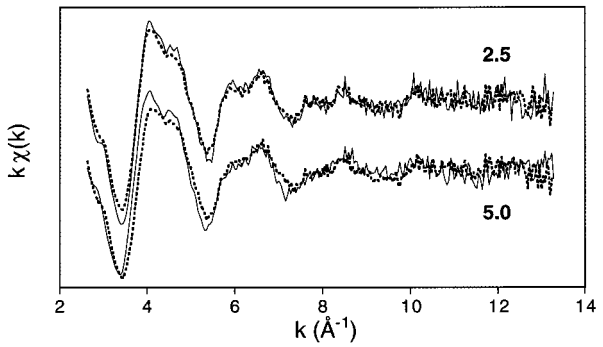

Figure 9. Comparison of the experimental EXAFS spectra (full lines) recorded at the Cu K edge for doped (2.5 and 5.0 mol %) SnO_2 xerogels with weighted linear combinations (dot lines) between the experimental EXAFS spectra for doped (0.7 mol %) and grafted samples fired at 300 °C for 30 min.

the decrease of the intensity of nearest tin neighbors, in particular those located along [111], gives rise to an intensity reduction of the sharp pointed first EXAFS oscillation and a loss of the structured shape for the others EXAFS oscillations. Furthermore, the comparison between the experimental spectrum of the grafted sample and the simulation of superficial substitution sites shows that the hypothesis of formation of a chemically adsorbed layer or of a nonhomogeneous solid solution near the surface can be distinguished.

These results show that by using copper as a local probe the EXAFS technique becomes a powerful tool to distinguish between inner or outer sites for copper with respect to the surface.

4.2. Effect of Dopant Concentration. The set of results above related shows that the structural evolution of Cu-doped SnO_2 xerogels is dependent on doping concentration. The increase of the amount of adsorbed water and the decrease of the linear shrinkage verified below 110 °C, as the amount of copper increases from 0.7 to 5% (Figure 1), indicate some changes on the characteristics of the crystallite surface. In fact, the observed shrinkage is generally attributed[27] to the increase in surface energy caused by desorption of water and the consequent increase of the capillary pressure. The decrease of capillary strain as the copper concentration increases may be due to the decrease of the surface energy by the presence of copper adsorbed on the surface of pore walls or to the increase of the stiffness of the particulate xerogel network due to the segregation of copper in the neck between particles. In this case, the copper rich secondary phase acts as a binder, increasing the contact area between particles. The first hypothesis is in agreement with the EXAFS and XRD results, as discussed below.

Namely, the comparison between the EXAFS signals and the simulation of lattice sites (Figure 8) allows one to conclude that in the 0.7% copper doped xerogel, the copper is in a substitutional solid solution. For samples doped with higher concentrations, the EXAFS signal shows a mixture between the copper in solid solution and copper adsorbed at the surface, since we can reproduce these EXAFS signals by a linear combination between the experimental spectra of the 0.7% doped copper xerogel and the grafted sample as shown in Figure 9. The best combinations to reproduce the experimental spectra were achieved by using a ponderation factor of 0.4:0.6 and 0.2:0.8 for samples doped with 2.5 and 5% copper, respectively. This indicates that the limit of solubility of copper in the cassiterite nanocrystals is around 1%. Corroboration of this comes from previous SAXS analysis,[9] which shows the presence of a rough surface due to islands of copper atoms for SnO_2 xerogels containing doping higher than 0.7 mol %. This limit of solubility is 10 times lower than the nominal doping for SnO_2 gels reported recently,[13] suggesting that the amount of incorporation is a function of the conditions of coprecipitation used in the sol−gel process. However, these unfired xerogels constitute a metastable solid solution, and a demixing with consequent copper segregation at the surface of the crystallite was observed during heating.[13] In fact the comparison of ab initio calculations (Figure 8) and experimental EXAFS spectra recorded for the 0.7 mol % sample at different firing temperature for 30 min (Figure 6) evidences a progressive migration of copper from the innermost substitutional site toward the superficial sites for $T > 300$ °C.

Interesting technological aspects emerging from the above discussion are (i) copper adsorbed at the surface helps to decrease the capillary strain and thereby hinders the formation of microcracks as previously suggested by SAXS analyses,[9] favoring the preparation of monolithic bodies, and (ii) the coprecipitation method produces xerogels characterized by a nonhomogeneous distribution of copper in the xerogel for copper concentrations higher than the limit of solubility determined in this work (1%), which is undesirable for the use of these materials as gas sensors or catalysts. For these applications, the grafted method is the best one, leading to more homogeneous copper distribution at the surface of crystallites, which favors the catalytic selectivity.[13]

4.3. Effect of Firing. The microstructural evolution of undoped and doped xerogels with increasing temperature presents the well-reported behavior of crystallite growth attributed to grain coalescence observed for nano-[8,9,11−13] and microcrystalline[1,7] SnO_2 based ceramics. Nevertheless as the mechanisms responsible of this process are not well-known, the discussion of the experimental results presented in this section will be focused on clarifying the key steps controlling the crystallite growth, first at the early time period of sintering, second at the later one.

The microstrain values of dried samples (Figure 2) are comparable to the ones observed for cold deformed alloys[28] in which the excess of elastic energy is released during annealing by recrystallization. The relaxation of microstrain, the growth of the crystallite with temperature, and the exothermic peak observed by DTA (Figure 1) indicate that a similar recrystallization process occurs in SnO_2 xerogels. Examination of the microstrain as a function of the copper concentration evidences two contributions to the lattice deformation, the first one driven by stress inside the crystallite, the second driven by surface

distortion. This conclusion arises from results obtained at [110] for samples treated at $T < 320$ °C where the largest strain value is observed for the 0.7% copper doped xerogel for which we note the formation of a solid solution and the smallest one for the copper grafted xerogel. Consequently the observed crystallite growth due to recrystallization could be induced by both lattice defect mobility and surface processes. Nevertheless, the strong crystallite growth occurs only after the removal of superficial hydroxyl groups ($T > 400$ °C), which is evidenced by the mass loss between 150 and 450 °C. This indicates that olation reactions involving OH groups at the surface of adjacent crystallites play a minor role in crystallite growth. On the other hand, the pronounced crystallite growth for the substitutional solid solution (0.7 mol % doped xerogel) fired between 250 and 350 °C shows that the crystallite growth process has a significant contribution of lattice diffusion. This process is not associated with the copper migration process since EXAFS results (Figure 6) show that, in this temperature range, copper has the innermost position in the crystallite. Hence, the increase in lattice diffusion, due to the high oxygen vacancy concentration of a copper substitutional solid solution, should govern the crystallite growth. This process is unusual for low-temperature sintering,[29] but in the case of nanocrystalline materials for which the diffusion length from the bulk to the surface is small, this bulk process can dominate the surface ones. It is important to note that the resulting structure is so stressed that a recrystallization occurs between 350 and 450 °C (evidenced in Figure 2 by a decrease of the crystallite size) concommitantly with the migration of copper from the innermost position to the superficial substitutional site. At higher temperatures, the increased amount of copper adsorbed at the surface of crystallites, which covaries with the copper doping concentration, decreases the crystallite boundary mobility, hindering crystallite growth for the early time period of firing.

For the later time period of sintering, the crystallite size does not depend on the copper concentration (Figure 3) for concentrations lesser than 2.5 mol %. In fact, copper migration with the increase of temperature clearly evidenced for the 0.7 mol % sample is verified whatever the copper concentration. Due to this diffusional process, all the samples have a copper rich surface which hinders the crystallite growth. For copper concentrations higher than 5 mol %, the EXAFS results (Figure 4) at the Sn K edge indicate that the crystallite size is governed by the amount of copper adsorbed at the crystallite surface.

5. Conclusion

The ab initio simulations of experimental EXAFS spectra show undoubtly that a metastable copper tin oxide substitutional solid solution has been formed by a sol−gel process for copper doping lower than 1 mol %. Above this limit the excess copper is adsorbed at the surface of the crystallite. Under the effect of temperature, the copper moves from the substitutional inner sites to the surface, giving rise to a nonhomogeneous solid solution for samples containing copper concentrations up to the limit of solubility. A similar phenomenon is observed for higher dopant concentrations but the excess copper remains adsorbed at the external surface. The presence of the adsorbed copper modifies the surface properties, inhibiting the shrinkage associated with water loss and with the olation reactions from hydroxo groups at the surface of crystallites. As a consequence, crack-free monolithic bodies are easily obtained from copper doped SnO_2 xerogels (5 mol %). The formation of a substitutional solid solution leads to a very stressed structure which induces a recrystallization process near 320 °C; this is the first driving force for crystallite growth. Nevertheless, the presence of copper at the surface reduces the surface distortion near the surface, hindering crystallite growth.

Acknowledgment. The authors acknowledge, with thanks, the help of Professor A. Michalowicz for fruitful discussions. This work has been financially supported by the CNPq and FAPESP (Brazil) and by a CAPES/COFECUB cooperation program between Brazil and France.

Supporting Information Available: Figure 1S showing in situ X-ray powder diffraction patterns obtained during heating of undoped SnO_2 xerogel and Table 1S containing all the structural parameters determined by EXAFS at the Sn K edge (2 pages). See any current masthead page for ordering information and Internet access instructions.

References and Notes

(1) Yamazoe, N.; Kurokawa, Y.; Seiyama, T. *Sens. Actuators* **1983**, *4*, 283.

(2) Lalauze, R.; Pijolat, C. *Sens. Actuators* **1984**, *5*, 55.

(3) MacKawa, T.; Tamaki, J.; Miura, N.; Yamazoe, N. *J. Mater. Chem.* **1994**, *4*, 1250.

(4) Blunden, S. J.; Cusak, P. A.; Hill, R. In *The Industrial Uses of Tin Chemicals*; Royal Society of Chemistry: London, l985; Chapter 9.

(5) Zaharescu, M.; Mihaiu, S.; Zuca, S.; Matiaaovsky, K. *J. Mater. Sci.* **1991**, *26*, 1666.

(6) Varela, J. A.; Whittemore, O. J.; Longo, E. *Ceram. Int.* **1990**, *16*, 177.

(7) Dolet, N.; Heintz, J. M.; Rabardel, L.; Onillon, M.; Bonnet, J. P. *J. Mater. Sci.* **1995**, *30*, 365.

(8) Xu, C.; Tamaki, J.; Miura, N.; Yamazoe, N. *J. Mater. Sci.* **1992**, *27*, 963.

(9) Brito, G. E. S.; Santilli, C. V.; Pulcinelli, S. H.; Craievich, A. F. *J. Non-Cryst. Solids* **1997**, *217*, 41.

(10) Briois, V.; Santilli, C. V.; Pulcinelli, S. H.; Brito, G. E. S. *J. Non-Cryst. Solids* **1995**, *191*, 17.

(11) Brito, G. E. S.; Briois, V.; Pulcinelli, S. H.; Santilli, C. V. *J. Sol-Gel Sci. Technol.* **1997**, *8*, 269.

(12) Brito, G. E. S.; Pulcinelli, S. H.; Santilli, C. V.; Craievich, A. F *J. Appl. Crystallogr.* **1997**, *30*, 664.

(13) Davis, S. R.; Chadwick, A. V.; Wright, J. D. *J. Phys. Chem. B* **1997**, *101*, 9901.

(14) Matar, K.; Zhao, D.; Goldfarb, D.; Azelee, W.; Daniel, W.; Harrison, P. G. *J. Phys. Chem. B* **1995**, *99*, 9966.

(15) Enzo, S.; Parrish, W. In *Advances in X-ray Analysis*; Plenum Press: New York, 1984; Vol. 27, p 37.

(16) Teo, B. K. *EXAFS: Basic Principles and Data Analysis*; Springer-Verlag: Berlin, 1986.

(17) Michalowicz, A. *EXAFS pour le Mac, Logiciels pour la Chimie*; Société Française de Chimie: Paris, 1991; p 102.

(18) Serrini, P.; Briois, V.; Horrilo, M. C.; Traverse, A.; Manes, L. *Thin Solid Films* **1997**, *304*, 113.

(19) Åsbrink, S.; Norrby, L.-J. *Acta Crystallogr. B* **1970**, *26*, 8.

(20) McKale, A. G.; Veal, B. W.; Paulikas, A. P.; Chan, S. K.; Knapp, G. S. *J. Am. Chem. Soc.* **1988**, *110*, 3763.

(21) Andreatta, D.; Cepparo, A.; Colavita, P. E.; Fonda, E.; Michalowicz, A.; Vlaic, G., submitted to J. Synchrotron Radiation.

(22) Lytle, F. W.; Sayers, D. E.; Stern, E. A. *Physica B* **1989**, *158*, 701.

(23) Mustre De Leon, J.; Rehr, J. J.; Zabinsky, S. I.; Albers, R. C. *Phys. Rev. B* **1991**, *44*, 4146.

(24) Sharygin, L. M.; Gonchar, V. F.; Barybin, V. I. *IZV. Akad. Nauk SSSR, Neorg. Mater.* **1981**, *17*, 1804.

(25) Orel, B.; Lavrencic-Stangar, V.; Crnajack-Orel, Z.; Bukovec, P.; Kosec, M. *J. Non-Cryst. Solids* **1994**, *167*, 272.

(26) Fang, G.; Liu, Z.; Zhang, Z.; Hu, Y.; Ashur, I. A.; Yao, K. L. *Phys. Stat. Sol. (a)* **1996**, *156*, 15.

(27) Brinker, C. J.; Scherer, G. W. *Sol−Gel Science: The Physics of Sol−Gel Processing*; Academic Press: San Diego, 1990.

(28) Cohen, J. B.; Hilliard, J. E. *Local Atomic Arrangement Studied by X-ray Diffraction*; Gordon and Breach: New York, 1965; Chapter 9.

(29) Chiang, Y. M.; Binier, D. P., III; Kingery, W. D. *Physical Ceramics: Principles for Ceramic Science and Engineering*; John Wiley and Sons Inc.: New York, 1997; Chapter 5.